2014

Structural Analysis Of Bulky Thiolate-Protected Gold Nanomolecules

David Walton Crasto
University of Mississippi

STRUCTURAL ANALYSIS OF BULKY THIOLATE-PROTECTED GOLD NANOMOLECULES

Thesis
presented in partial fulfillment of requirements
for the degree of Master of Science
in the Department of Chemistry and Biochemistry
The University of Mississippi

by

DAVID W. CRASTO, JR.

July 2014

ABSTRACT

Routine preparation of thiolate-protected gold nanomolecules involves, most commonly, straight-chain organic thiolate ligands for which the sulfhydryl 'head' group is bound to a primary carbon atom. The primary connectivity of these sulfur atoms, such as for the case of *n*-hexanethiol and phenylethanethiol, allows for even packing, and the relative ease of formation of gold-thiolate oligomers about the surface monolayer in the formation of Au-SR bonds. Moreover, these straight-chain ligands routinely support the formation of an icosahedron-based series of core-size gold nanomolecules. Within this series of nanoparticles, $Au_{25}(SR)_{18}$ and $Au_{38}(SR)_{24}$ are among the most commonly studied core-sizes; $Au_{25}(SR)_{18}$ is situated upon an Au_{13} icosahedron, and $Au_{38}(SR)_{24}$ upon two face-fused icosahedra which share three gold atoms to give an Au_{23} core structure. The investigation of the experimental results presented by the student in this thesis outlines the alteration of these icosahedron-based core geometries. Specifically, by varying the steric hindrance of the –R group for which the sulfur head group is bound, a heightened gold:thiol ratio is achieved. With the application of bulky ligands, most notably *tert*-butanethiol and 1-adamantanethiol, the underlying geometry is altered such that face-centered cuboidal (fcc), octahedron-based structures are favored.

These structures are defined by atomic compositions, predicted by mass spectrometry and confirmed by X-ray Diffraction methods, for which a fewer number of sulfur ligands are needed to stabilize the overall structure. This is best illustrated in the case of the $Au_{25}(S\text{-}C_2H_4)_{18}$ and the $Au_{30}(S\text{-}t\text{-}C_4H_9)_{18}$ nanomolecules; because both have the same number of stabilizing ligands, it is clear that the addition of five gold atoms to the composition is accompanied by a structural alteration. In this work, the research and discussion focuses on the structural alteration associated with the 3-dimensional atomic arrangement in employment of bulky ligands, with experimentally-dervived data acquired from mass spectrometry, UV-visible spectroscopy, and single-crystal X-ray Diffraction.

OBJECTIVES

The works and findings presented within this document that pertain specifically to the research project of the student are focused on the determination of the alteration in structure of gold nanomolecules when introducing bulky, sterically-demanding thiolate ligands in the synthetic scheme. The manner in which this is outlined is by first introducing the topic of transition metal-based nanostructures, and those structures of gold molecules for which are known and routinely studied. Based on this information, the application of bulky ligands, including our isolation of the green-gold $Au_{30}(StBu)_{18}$ gold molecule, are detailed in contrast from those common structures stabilized with routinely-studied ligands. Our work deducing the single-crystal X-ray structure and, therefore, the 3-Dimensional arrangement of the atoms, is explained and illustrated in chapter four. The determination of the $Au_{30}(StBu)_{18}$ structure by the student in this research project is of fundamental interest to the underlying aspects governing structural-acquisition in gold nanochemistry.

LIST OF ABBREVIATIONS

SR	thiol group
StBu	*tert*-butanethiol
tert-C_4H_9	*tert*-butanethiol
XRD	X-ray Diffraction
UV-vis-NIR	Ultraviolet-visible-Near Infared
MS	Mass Spectrometry
MALDI-TOF	Matrix-Assisted Laser Desorption/Ionization-Time of Flight
ESI	Electrospray Ionization
Au	Gold

ACKNOWLEDGEMENTS

I would like to thank Dr. Dass for all of his help and guidance since beginning working in his laboratory. I would also like to individually thank all of my fellow graduate students for all of their deeply-appreciated help and input over the years: Vijay Jupally, Praneeth Nimmala, Chanaka Kumara, Asantha Dharmaratne, and Nuwan Kothalawala. I would also like to give thanks to Dr. Hanuu Hakkinen and his post-doctoral fellow, Dr. Sami Malola, for their collaborative efforts in performing calculations and modeling theoretical designs. Additionally, I would like to thank Dr. Walter Cleland and Dr. Charles Hussey for bringing the Bruker Apex II diffractometer to the department.

LIST OF TABLES

LIST OF FIGURES

TABLE OF CONTENTS

Chapter **Page**

CHAPTER I: INTRODUCTION

The noble metals are transition-metal elements, and include the following: Ru, Rh, Pd, Ag, Os, Ir, Pt, and Au (Re is also associated in some instances). These are commonly referred to as "precious" metals, and are characteristically chemically inert, resistant to oxidation and corrosion under ambient conditions, non-radioactive, and quite expensive as well. Development of gold nanostructures is of fundamental interest across a broad range of scientific fields for the many wide range of applications, among which includes biomolecule sensors [2], catalysis [3], and drug delivery [4]. Thiolate-protected gold nano-'molecules' receive their name in light of the fixed composition pertaining to the number of gold atoms and thiol ligands, giving the overall chemical formula $Au_x(SR)_y$ where x=the number of Au atoms, and y=thiol ligands attached. The 'thiol' group is represented by '(SR)', where S denotes the sulfur atom of the sulfhydryl functional group, and R representative of an alkyl/aryl group attached to the sulfur 'head' group. Examples of these thiolate-protected gold nanomolecules includes $Au_{25}(SR)_{18}$ and $Au_{38}(SR)_{24}$, where the R-group can be varied between phenylethanethiol and hexanethiol. These are shown below, in figure 1, which illustrates the low degree of crowding about the carbon atom attached to the sulfur atom.

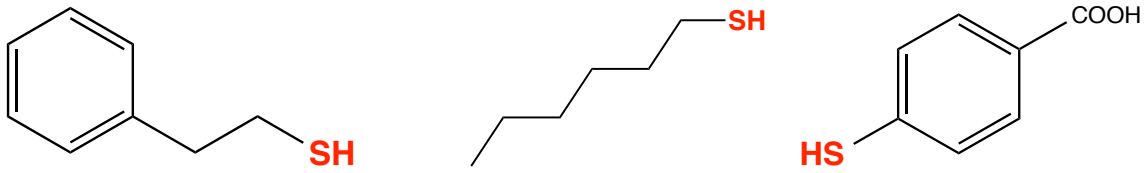

a. phenylethanethiol **b. *n*-hexanethiol** **c. *para*-mercaptobenzoic acid**

Figure 1. Structures of three routinely-employed thiolate ligands, both with primary connectivity of the carbon atom bound to the sulfur atom **a.** Structure of phenylethanethiol, with the chemical formula of $C_6H_5CH_2CH_2SH$ **b.** Structure of *n*-hexanethiol, with the chemical formula of $C_6H_{13}SH$ **c.** Structure of *para*-mercaptobenzoic acid, with the chemical formula of C_6H_4COOHS

In the procedural mechanisms for the synthesis of routinely studied Au nanomolecules, employing these straight-chain ligands leads to the formation of the routinely-observed compositions; among these includes $Au_{25}(SR)_{18}$, $Au_{38}(SR)_{24}$, $Au_{67}(SR)_{35}$, and $Au_{102}(SR)_{44}$. These are displayed in figure 2, which shows the MALDI-MS (Matrix Assisted Laser Desorption/Ionization-Time of Flight Mass Spectrometry) of the 1+ charge states pertaining to routinely studied compositions, displaying their large deviance in size (from $Au_{102}(SR)_{44}$ at ~27,500 Da and $Au_{67}(SR)_{35}$ at ~18,000 Da).

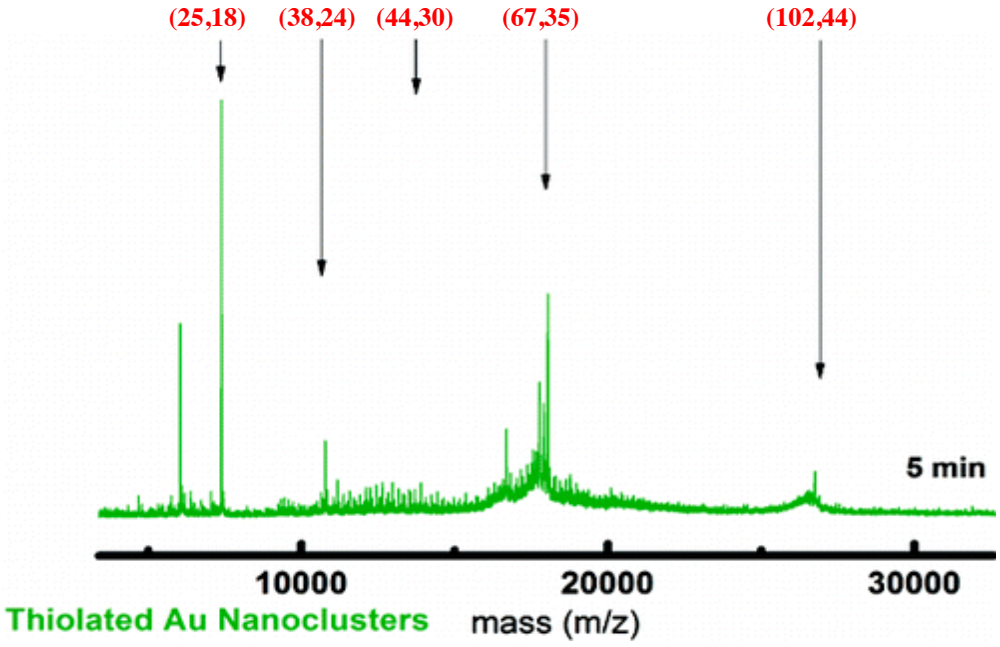

Figure 2. MALDI-TOF MS of phenylethanethiol stabilized Au nanomolecules, showing the measurable size difference between successive sizes as they increase in mass proportionally to their composition [1]. The (x,y) notations specifically denote the gold atoms and thiolate ligands comprising the composition, where x=number of Au atoms and y=number of organic thiolate ligands

With a primary connectivity of the carbon atom to the sulfur of the sulfhydryl 'head' group, these routine structures and their 3-Dimensional atomic arrangement have been elucidated experimentally as fixated upon icosahedron-based Au cores surrounded by an external monolayer with the Au-SR coordination [5,6]. $Au_{102}(p\text{-MBA})_{44}$, stabilized by *para*-mercaptobenzoic acid and thereby making it soluble in water, is shown in figure 3 [7]. This particular structure, elucidated experimentally, is fixated upon an Au_{79} decahedron with two dimeric staples as in the case of $Au_{25}(SR)_{18}$ and $Au_{38}(SR)_{24}$. There are, additionally, nineteen 'monomeric' $Au(SR)_2$ staples coordinating on the surface that, in conjunction with the six ligands located in dimeric staples, comprise the remaining thirty-eight ligands which give the total of fourty-four present on the surface monolayer.

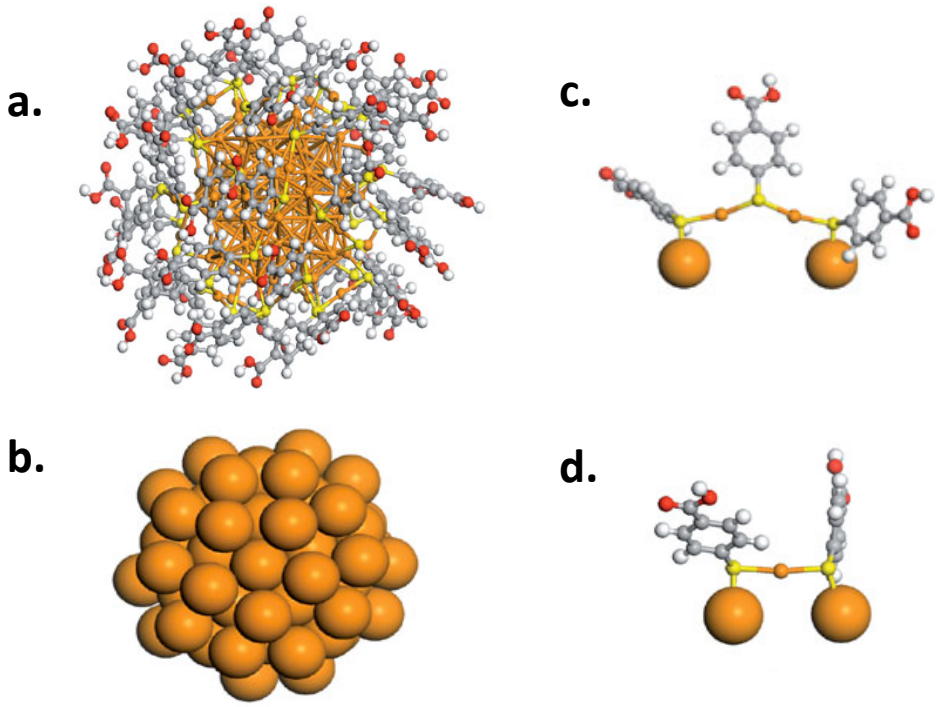

Figure 3. Structure of the $Au_{102}(p\text{MBA})_{44}$ Au nanomolecule. **a.** Total Structure, including hydrogen atoms **b.** Au_{79} decahedron core **c.** $Au_2(SR)_3$ dimeric staple moiety **d.** $Au(SR)_2$ monomeric staple moiety [8]

The structure of the $Au_{25}(SC_2H_4\text{-}Ph)_{18,}$ shown in figure 4, was elucidated experimentally using X-ray crystallography in 2008 and revealed an Au_{13} icosahedron gold core surrounded by an external monolayer. This monolayer houses six dimeric staples, each possessing two gold atoms and three phenylethanethiol ligands in coordination on the surface; this gives rise to the additional twelve gold atoms totaling to twenty-five gold atoms and eighteen phenylethanethiol ligands. The Au_{13} icosahedron consists of a central Au atom that forms twelve Au-Au bonds to each of the additional twelve Au atoms forming the vertices of the icosahedron, possessing an average bond length of 2.79 Å. This is smaller when compared with the Au-Au bond length in the bulk, which has been found to extend 2.88 Å.

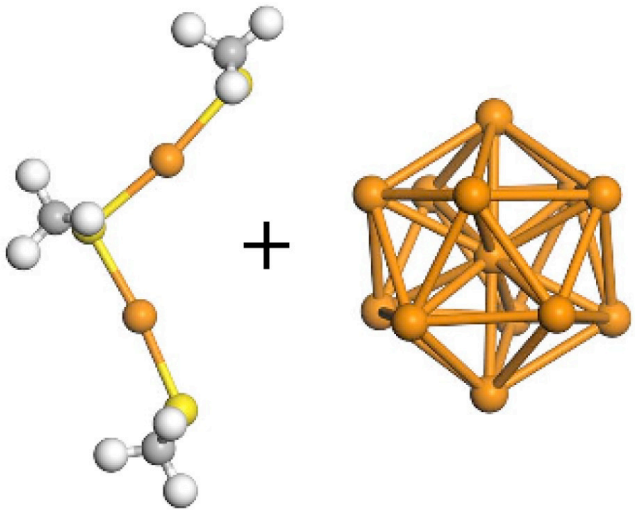

Figure 4. Two different layers of the $Au_{25}(SR)_{18}$ nanomolecule. Displayed on the left is the connectivity of the dimeric staples, with the two gold atoms shown in orange accompanied by the three methanethiol ligands with the S atom in yellow. Shown on the right is the Au_{13} icosahedron, whereby twelve Au atoms form the vertices of the geometrical architecture and each singly-bond to the central Au atom, of which there are twelve bonds extending from to these twelve vertice-Au atoms

In 2012, Jin and co-workers [9] reported their findings pertaining to the total structure of the $Au_{36}(STBBT)_{24}$ nanomolecule (figure 5), where TBBT=4-*tert*-butylbenzene thiol. The gold core underlying the entire structure is fixated into an Au_{28} fcc-kernel, a remarkable change from that of the previously-observed icosahedron based Au nanomolecules. Distributed about this Au_{28} kernel are four dimeric staples, each with two Au atoms to give the overall total of thirty-six Au atoms. In addition to the twelve ligands found in coordination, there are twelve novel 'bridging' thiolate ligands found binding directly to the Au_{28} core. This gives rise to the overall twenty-four ligands in the composition.

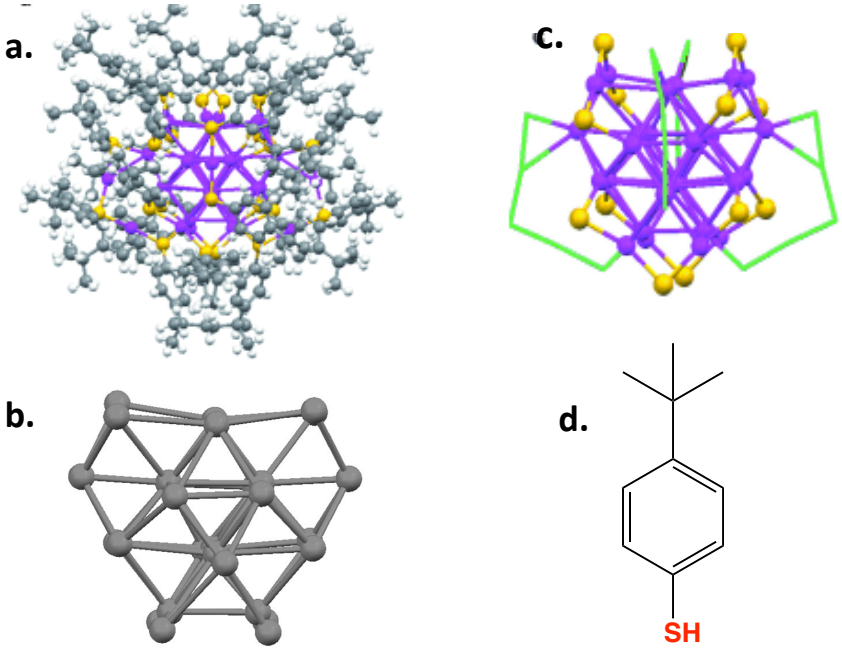

Figure 5. Structure of the $Au_{36}(STBBT)_{24}$ nanomolecule. **a.** Total structure of the $Au_{36}(STBBT)_{24}$ nanomolecule, with hydrogen atoms included **b.** Au_{28} fcc-kernel **c.** Orientation of the four dimeric staples (shown in green), with two extending longitudinally in a perpindicular fashion to the other two for which extend laterally. Additionally, the Au-S coordination with respect to the bridging thiolates is indicated by the yellow sulfur atoms **d.** Connectivity of the 4-*tert*-butylbenzene thiol ligand used to stabilize the entire nanomolecule

Based on single-crystal X-ray diffraction experiments, it is reasonable to conclude that the employment of the routine straight-chain alkanethiol and arenethiol ligands such as, respectively, *n*-hexanethiol and phenylethanethiol, leads to routinely observed nanoparticles oriented three-dimensionally about icosahedron-based central gold cores. As discussed previously, $Au_{25}(SCH_2CH_2Ph)_{18}$ is constructed about an Au_{13} icosahedron, where six dimeric staple moieties are observed coordinating about the core. $Au_{38}(SCH_2CH_2Ph)_{24}$ on the other hand, also included among those referred to as 'routinely observed', is built around an Au_{23} face-fused icosahedron. Briefly, two Au_{13} icosahedra share three gold atoms in their midplane (13+13=26-3**shared*=23) to give the total of twenty-three gold atoms housed in the central core. Additionally, there are three monomeric $Au(SCH_2CH_2Ph)_2$ staples coordinating about the three gold atoms shared along the surface of the midplane as well as six dimeric staples in the case of $Au_{25}(SCH_2CH_2Ph)_{18}$. With the 2012 report of the structural elucidation pertaining to $Au_{36}(STBBT)_{24}$ describe above, the researchers were left uncertain to the reason for the structural alteration in going from the icosahedron-based structure to that of the fcc-based cuboctahedron nanomolecules; it was proposed, however, that the effects are due in part to resonance more so than the bulkiness of the ligand itself.

CHAPTER II: BULKY-LIGAND STABILIZED AU NANOMOLECULES

Tracy and co-workers [10] sought to demonstrate effects in the products formed in nanomolecules formed in crude-product syntheses solely attributable to increasing sterics on the monolayer. This was carried out in the presence of three ligands shown in figure 6, includes *n*-hexanethiol, cyclohexanethiol, and adamantanethiol; it was shown that increasing steric crowding on the surface monolayer ultimately gives rise to nanoparticles with compositions (assigned based on MALDI-TOF MS) representative of heightened Au:thiol ratios. Among these new compositions reported include $Au_{30}(SAd)_{18}$, $Au_{39}(SAd)_{23}$, and $Au_{67}(SCy)_{30}$ where SAd=1-adamantanethiol and SCy=cyclohexanethiol (shown in figure 6). Their results with these two particular ligands, in conjunction with *n*-hexanethiol (also shown in figure 6), indicated a shortened size-growth range that terminals with smaller sizes that do not exceed the ~20,000 Da mass-range. Additionally, their results showed a mixture of nanoparticles in the crude-product synthesis for which are stabilized with 1-adamantanethiol and cyclohexanethiol have a smaller average size, as well as shortened-size range between based on their smaller standard deviation T.E.M.-measurements between successive sizes as compared with the *n*-hexanethiolate crude product which revealed a larger average sizes with increased standard deviation (larger separation) between these sizes.

This shortened-size range between nanoparticles in the bulky-ligated products is indicative of difficulties in isolation of a pure material in order for characterization. Though the assigned compositions were based on the hard-ionization of the MALDI-TOF MS laser, the compositions reflected, more importantly, an alteration of geometry in the Au nanomolecules generated in a sterically-demanding environment. This is illustrated with the compositional assignment of $Au_{30}(AdmSH)_{18}$ in comparison with that of the routinely-studied $Au_{25}(SR)_{18}$; with the addition of five Au atoms in the assignment, it is clear that the manner in which they are adopted into the geometrical framework indicates a complete alteration of the three-dimensional architecture, starting from the central Au core and working out to the monolayer environment. Moreover, there was no $Au_{25}(SR)_{18}$ observed in the product points to the fact that perhaps its formation is disfavored due to being too sterically crowded.

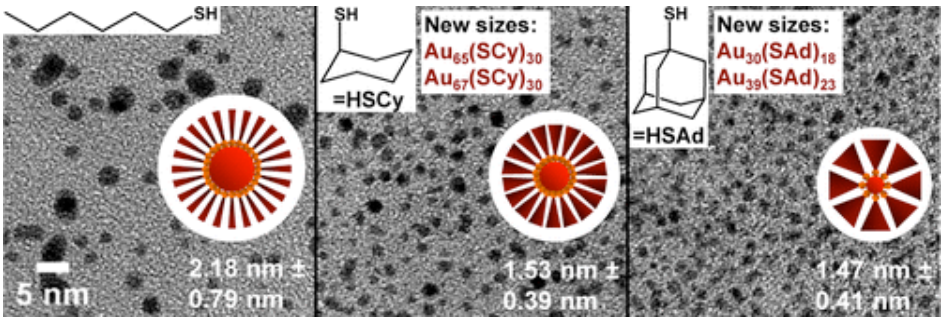

Figure 6. High-Resolution Transmission Electron Microscopy images of Au nanomolecules generated in *n*-hexanethiol, cyclohexanthiol, and 1-adamantanethiol, accompanied by the skeletal structures of the respective ligands. Shown on the left is the *n*-hexanethiol stabilized nanomolecules, with the largest average size among the products formed, as well as the highest standard deviation in the sizes of products formed (increased separation in size-gap). In the middle is cyclohexanethiol, with the median average size among the three ligands. 1-adamantanethiol, predicted to introduce the highest degree of steric crowding among the three ligands & shown on the right, revealed the smallest average sizes.

Tsukuda and co-workers [11] reported on the first isolation and characterization of a pure product stabilized by a bulky ligand. Their purification scheme leads to the isolation of pure $Au_{41}(S\text{-}Eind)_{12}$, where S-Eind=1,1,3,3,5,5,7,7-octaethyl-*s*-hydrindacene-4-thiol. Their synthesis involved ligation of this respective thiolate complex, synthesized by the group as part of the study, onto preformed clusters stabilized by PVP (polyvinyl-pyridine). With the employment of MALDI-TOF MS, the researchers were able to assign the precise composition of forty-one gold atoms and twelve 1,1,3,3,5,5,7,7-octaethyl-*s*-hydrindacene-4-thiol ligands. X-ray Photon Spectroscopy (XPS) measurements pertaining to Au-Au bond lengths, as well as Au-S lengths, led to their conclusion that all of the gold atoms are housed within an Au_{41} core oriented in a 'pyramidal' geometry (figure 7a), with the twelve Eind-SH ligands distributed about the pyramid. High-Resolution T.E.M. microscopy provided further evidence to this inference, whereby in figure 7b it is shown that some of the particles detected are of a pyramidal appearance in the image collected.

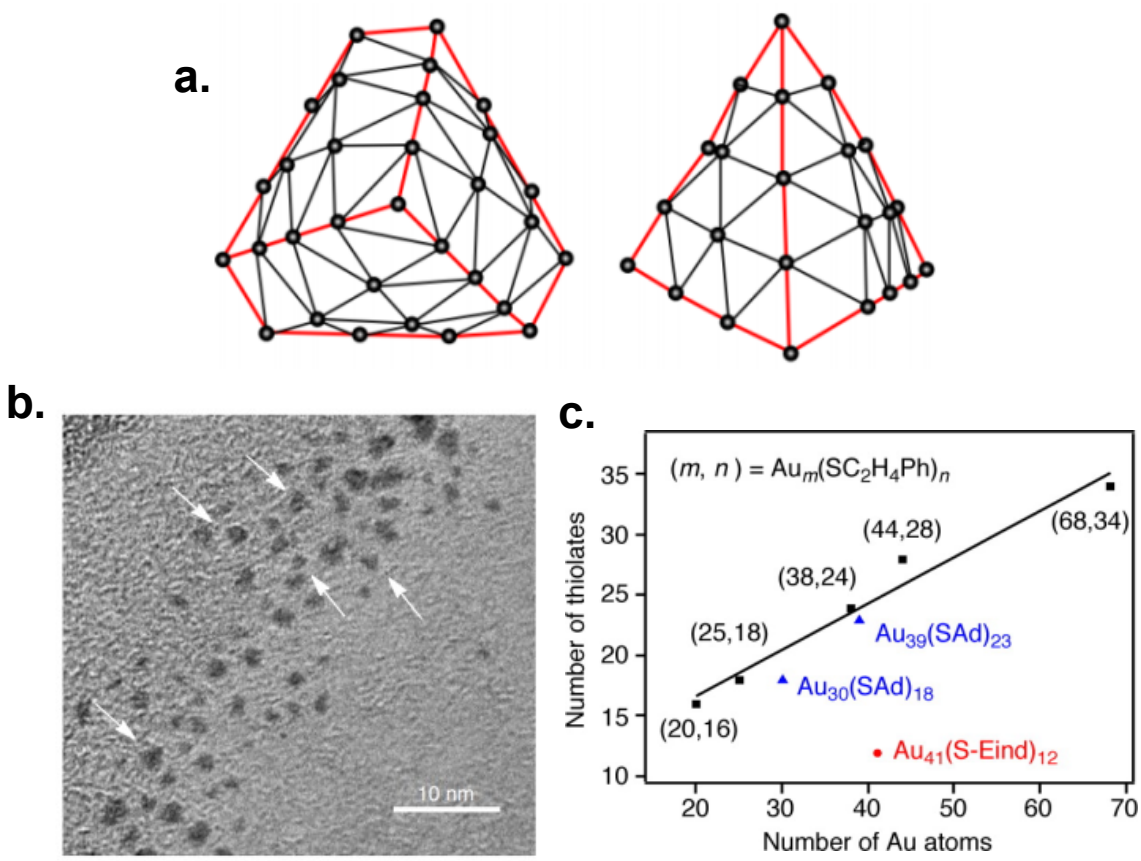

Figure 7. Data measurements collected by Tsukuda and co-workers with regards to the sterically-demanding $Au_{41}(S\text{-}Eind)_{12}$ nanomolecule. a. Pyramidal Au_{41} core, constructed in light of results given by XPS measurements b. High-Resolution T.E.M. showing the additional evidence for the pyramidal-appearance of the nanomolecule. c. Plot showing the deviation in Au:thiolate ratio for the bulky-ligated nanomolecules.

Motivated by the works of Tracy and Tsukuda describe on the proceeding pages, our work [12] involved the use of *tert*-butanethiol which led to synthesizing and separating pure $Au_{30}(StBu)_{18}$, where StBu=*tert*-butanethiol (2-methyl-2-propanethiol, shown in figure 8 below). The synthesis is described in more detail in Ch. 3; briefly, a one-phase synthesis in a THF medium of 1:3 Au:*tert*-butanethiol mole ratio is stirred (in the absence of any counterion) at 450 rpm under ambient conditions for fifteen minutes, prior to additon of sodium borhohydride ($NaBH_4$), thereby reducing the light yellow Au(I)-S-*t*Bu complex to a black mixture of Au^0 nanomolecules. The product is then let stir for an hour after the reduction and proceeds to undergo thermochemical treatment under aggressive conditions (high temp, excess ligand) for three hours to collect the most thermodynamically-stable product. The thermochemical (etching) product is then added to a Size-Exclusion Chromatogram (S.E.C.) column, whereby the pure material is observed to elute in a final green band (figure 8).

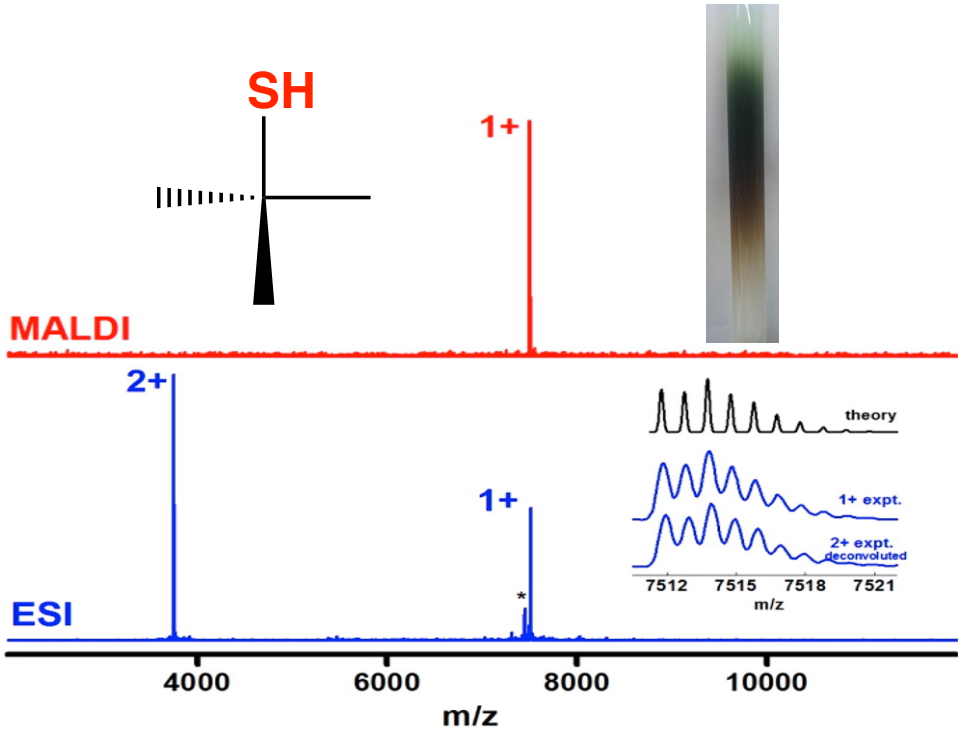

Figure 8. Mass-Spec. composition assignment of $Au_{30}(StBu)_{18}$ green-gold nanomolecules. Shown on top in red is the MALDI-MS positive mode data collection of the green band in the S.E.C. column (top left) eluting last, displaying the high purity in light of the sole presence of the molecular ion for the $Au_{30}(StBu)_{18}$. The bottom spectrum (shown in blue) is the ESI-MS positive mode high-resolution mass spectrum of the green band containing pure green-gold $Au_{30}(StBu)_{18}$, displaying the 1+ and 2+ charge states at m/z=7511.7 and 3756.9, respectively. Shown in the inset (bottom right) are the isotopic distribution patterns for the 1+ and 2+ (deconvoluted) experimental charge states (blue) accompanied by the theoretical pattern shown on top in black. Additionally, the structure of *tert*-butanethiol, illustrating the tertiary-connectivity of the carbon atom attached to the sulfur head group is shown (top left)

The $Au_{30}(StBu)_{18}$ molecule has a distinct green color both in solid state and in solution, which is of fundamental interest in optics. Shown in figure 9, the optical absorption spectrum (left) displays a strong absorption peak at 620 nm. Additionally, the transmission of 520-570 nm light corresponds to the transmission of green light, thus giving rise to the respective appearance of the nanomaterial. There is also a portion of the red (630–740 nm) and blue (440–490 nm) regions within the visible-light that are being absorbed. This leads to the green color (inset, Figure 9-left) of the $Au_{30}(StBu)_{18}$ green-gold molecule. Shown on the right is the photon-energy plot compared with the spectrum for chlorophyll, a naturally-occurring biological pigment with a green appearance, also known to absorb light and carry out photosynthesis; the optical band gap is approximated by the tangent-line drawn through the x-axis (photon energy, in electron volts-eV) of the first excitation peak, and was found to be 1.76 eV. The differences in appearance with regards to to the green color of $Au_{30}(StBu)_{18}$ and the brown color of $Au_{25}(SR)_{18}$ is due to an alteration in the atomic structure.

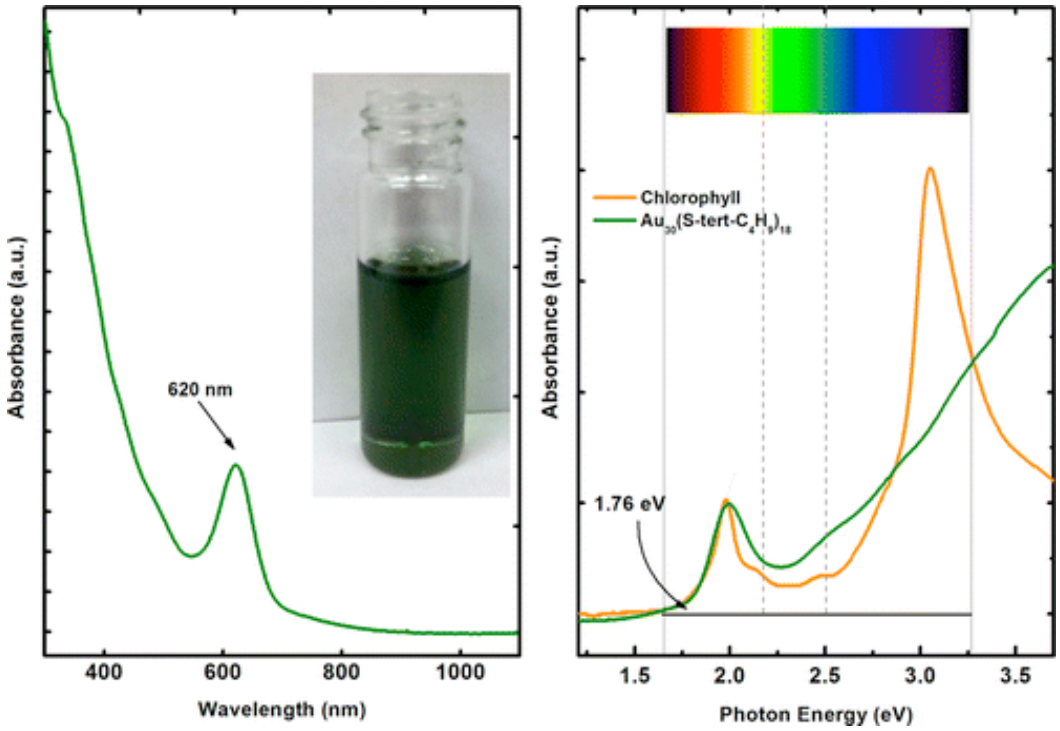

Figure 9. UV-vis-NIR of the $Au_{30}(StBu)_{18}$ green-gold nanomolecule (left) and corresponding photon energy (right) compared with chlorophyll. The absorption valley in the 520-570 nm range, in conjuction with the peak of absorbance corresponding to 620 nm and absorbance of red (630-740 nm) and blue (440-490 nm) light give rise to the green appearance (inset, left). The photon energy plot, shown on the right, illustrates the 1.76 eV bandgap based upon tangential-line approximation from the absorbance spectrum alongside the spectrum for chlorophyll. All spectra for chlorophyll and $Au_{30}(StBu)_{18}$ were collected in toluene as the solvent

In order to account for the compositional assignment, 1-adamantanethiol was also employed in the synthesis. The differences in mass of the 2+ charge states multiplied by a factor of two and then divided by the difference in mass of the two ligands gives rise to the total number of thiolate ligands present on the surface. Using this formula, the ESI-MS positive mode spectrum of the respective composition stabilized by *tert*-butanethiol (green) and 1-adamantanethiol (red) in figure 10a shows the conclusive thirty gold atom, eighteen thiolate ligand assignment for the green-gold composition. Powder X-ray diffraction (figure 10c, top right) shows a predominance of sharp, low angle peaks indicative of a densely packed, nano-crystalline material. This rigid surface environment, in conjunction with the heightened metal/ligand ratio and the absence of any $Au_{25}(SR)_{18}$ in the crude mixture, suggest the structure of the ligand (and, as a result, the steric crowding) functions as the underlying driving-force behind the establishment of a particular three-dimensional geometrical assembly in space. Increasing the laser intensity in MALDI-TOF MS (figure 10b) shows the ease of fragmentation associated with the rise. Positive and Negative Differential Pulse Voltammetry (DPV) Electrochemical measurements, shown on the bottom right in figure 10d, revealed inconclusive results; however, the electrochemical gap was reproducibly measurable, and determined to be 1.768 V. This slight difference greater than the optical band gap (1.76 eV from optical absorption studies) is expected for the charging energy of the material.

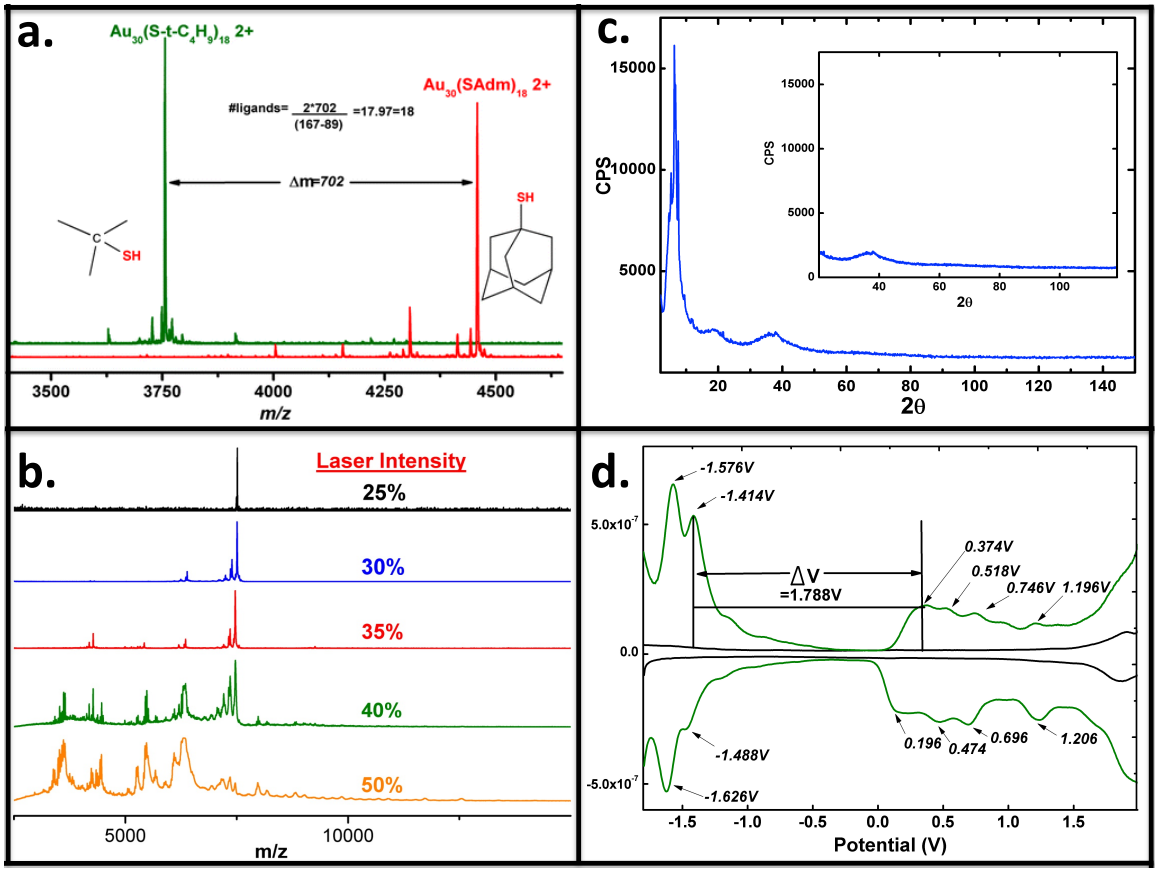

Figure 10. Compositional Assignment and Characterization via four modes of instrumentation: ESI-MS, MALDI-TOF MS, Powder X-ray diffraction, and DPV. **a.** Further evidence of the composition based on differences in mass of the 2+ charge states given by the employment of two ligands, *tert*-butanethiol and 1-adamantanethiol **b.** MALDI-TOF MS positive mode spectrum, displaying the heightened sensitivity to the MALDI laser. **c.** Powder X-ray diffraction experiment, showing the sharp peaks in the low angle region indicative of a nano-crystalline core material. **d.** Differential-Pulse Voltammetry, correlating to the 1.76 eV optical bandgap via determination of a 1.768 electrochemical gap

Based on results presented by Tracy and co-workers' report using bulky adamantanethiol and cyclohexanethiol ligands, the fundamental foundation for understanding the behaviors of nanomolecules stabilized with bulky ligands by demonstrating characteristics solely attributable to the bulkiness of the ligand in the products formed. Among these included a smaller average size, sharpened size range between different sizes, and a heightened gold:thiol ratio. Tsukuda and co-workers' report of the $Au_{41}(S\text{-}Eind)_{12}$ nanomolecule correlated the results previously-reported by Tracy with respect to the heightened Au:thiol ratio. Successful efforts using X-ray Photon Spectroscopy, and further backed by High-Resolution T.E.M., suggest a pyramidal core housing all forty-one gold atoms, with the twelve Eind-SH ligands all bridging directly to the core. The report of the green-gold $Au_{30}(StBu)_{18}$ in our lab provided conclusive information pertaining to the composition using high-resolution isotopic modeling available via the employment of Electrospray Ionization Mass Spectrometry. However, none of the results provided the information highly valued and exclusively pertaining to single-crystal X-ray diffraction studies elucidating the three-dimensional arrangement of atoms in space.

CHAPTER III: SYNTHESIS AND METHODOLOGIES

a. *Crude Product Synthesis*

Synthesis of the $Au_{30}(StBu)_{18}$ green-gold nanomolecule is based upon a one-pot synthesis in THF, whereby 0.100 g (0.254 mmol) of $HAuCl_4*3H_2O$ is added to 25 mL of HPLC-grade tetrahydrofuran (THF) from *Fischer Scientific*. 0.712 mmol of *tert*-butanethiol (2-methyl-2-propanethiol, *Acros Organics*) is combined to give a 1:3 molar ratio of Au:thiol; the reaction mixture is let stir at 450 rpm for fifteen minutes. The prominent yellow appearance of the initial solution is observed to become a faint cloudy yellow after this time period. 0.100 g (2.50 mmol, 1:10 mole ratio) of Sodium borohydride, $NaBH_4$ (*Sigma Aldrich*), is then added in 5 mL of cold distilled H_2O instantaneously. The reaction mixture then turns black, an indication of the formation of nanomolecules upon the reduction to Au^0. This black mixture of nanomolecules, whose spectra is shown in blue at the top of figure 11, is then allowed to stir at 450 rpm for forty-five minutes to an hour. Once the stirring is complete, excess aqueous layer is first removed from the reaction mixture and, after which, the THF solvent is dried using rotary evaporation. Once complete, the product is then quenched with methanol and transferred via pipet to a 20 mL screw-cap vial and centrifuged at 3,500 rpm for four minutes. After pipetting off the methanol layer, which contains the excess *tert*-butanethiol ligand, methanol is then re-added and the process repeated two sequential rounds in order to remove all of the excess ligand prior to storage.

b. *Thermochemical Treatment*

After the crude product synthesis is complete, and the product is dried and washed of all excess ligand from the direct synthesis, 15 mg of the *tert*-butanethiol protected Au nanomolecules generated in step a. are added to 0.5 mL of Toluene and 1.5 mL of *tert*-butanethiol. The reaction mixture is then added to an oil bath at 80° Celsius and stirred at 200 rpm. After three hours of etching, the reaction mixture appears apparently green; letting the stir continue for another hour, totaling to four hours in oil overall, gives rise to a product for which is prominently green. Repeating the drying via rotary evaporation and cleansing in MeOH as described above, the 'etching' product contains predominantly $Au_{30}(StBu)_{18}$ as per the green appearance based on MALDI-TOF MS and ESI-MS measurements.

c. *Size-Exclusion Chromatography*

After drying and cleansing the product collected from the thermal etching described in part b., 0.2-0.3 mL of THF (HPLC) is added to the dried material which is subjected to an S.E.C. column. The dark green material can be observed separating into two bands (figure 8) in the column, whereby a brown-band containing larger materials separates below (i.e. moving faster through the beads) a light green band with pure $Au_{30}(StBu)_{18}$. The process is repeated a second time using the green fraction in order to remove all materials found in the bottom brown-band.

d. *Crystal Growth*

In order to crystallize the green-gold for X-ray studies, vapor diffusion was employed as the technique for crystal-growth. A small amount (~1.0 mg) of $Au_{30}(StBu)_{18}$ purified in the S.E.C. column is first dissolved in 1.5-2.0 mL of toluene for the soluble portion in a 4 mL screw-cap vial. This vial is then transferred to an ethanol bath within a larger 20 mL screw-cap vial, comprising the insoluble portion of the apparatus. After the cap is screwed on the 20 mL vial, the crystallization apparatus is then stored for 7-10 days in order to observe best crystal growth. After this time period elapses, brown rhombic plate-like crystals are observed via a polarizing microscope settled at the bottom of the insoluble layer.

e. *Equipment*

The size-exclusion chromatogram was composed of Biorad-SX1 beads. UV-visible absorption spectra were harvested on a Shimadzu UV-1601 in toluene as the solvent-media. MALDI-TOF MS were collected on a Bruker Autoflex 1 mass spectrometer in linear postive mode which uses a nitrogen laser with a 337 nm wavelength absorbed by DCTB co-dissolved and co-crystallized with the analyte acting as a matrix material. ESI-MS spectra were acquired on Waters SYNAPT HDMS instrument in HPLC grade THF solvent, without any additives present, as well as toluene with added ethanol. The instrument was calibrated using $Au_{38}(SC_2H_4Ph)_{24}$ ions, which are closer to the mass of $Au_{30}(SR)_{18}$.

Electrochemical measurements were perfomed on a CHI 620 instrument using 8 mg of title compound in 1.0 mL of anhydrous dichloroethane solution with 0.5 mM $TBAPF_6$ as supporting electrolyte under nitrogen atmosphere. Powder X-ray diffraction measurements were collected on a quartz sample-chip for which the product collected after S.E.C. is first dissolved in minimal amounts of dichloromethane and air-dried upon, followed by data collection on a Bruker D8 Advance. X-ray crystallographic data was collected on a Bruker Apex II Diffractometer, with a Molybdenum source (λ=0.71073 Å).

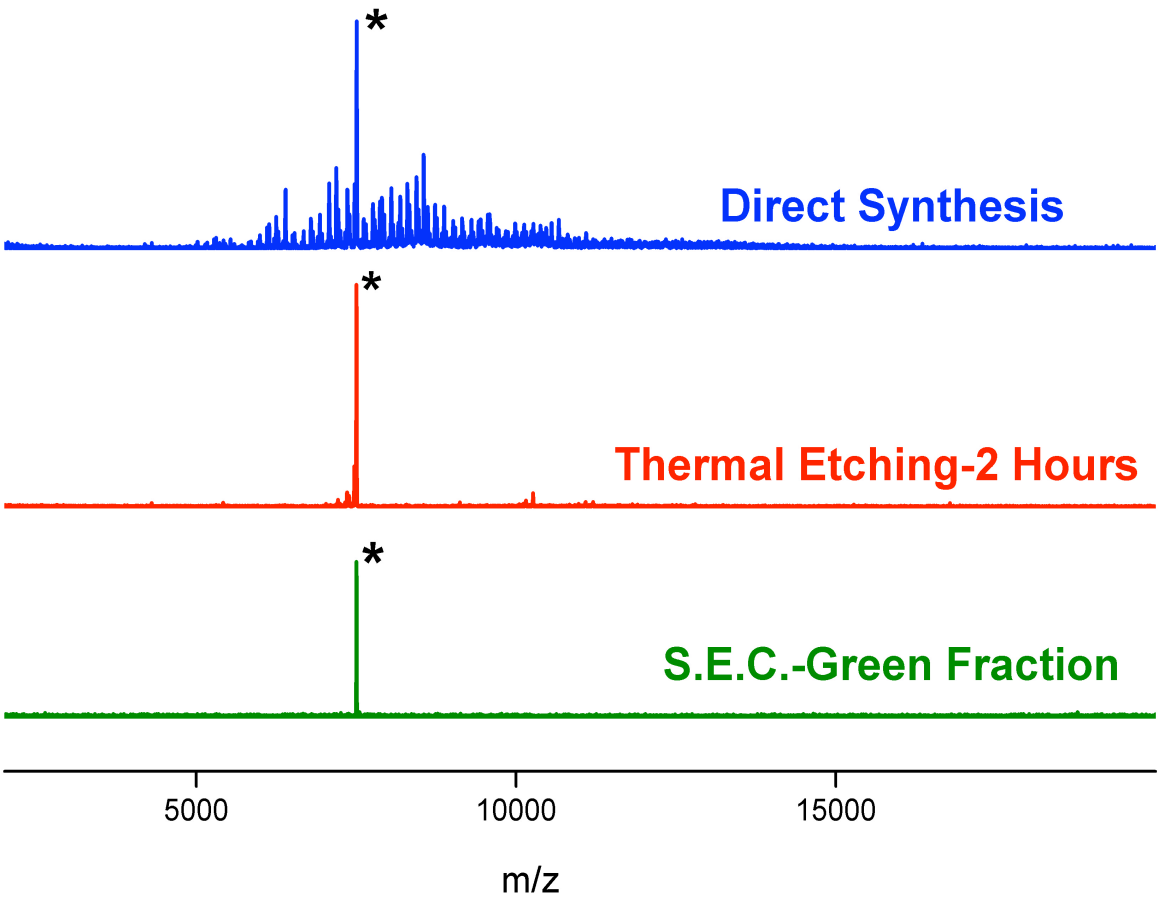

Figure 11. Purification scheme monitored by MALDI-TOF MS (positive mode), whereby the strength of the laser allows for accurate inferences made with regards to the purity of the material. The top blue spectrum represents the products collected after step a. on the previous page, displaying the sharpened size range between products formed. The thermal etching product, shown in the middle in red, is representative of the thermal etching product after two hours. It is clear that $Au_{30}(StBu)_{18}$ predominates in solution after which. The bottom green spectrum shows the purity of the $Au_{30}(StBu)_{18}$, with a single peak shown at an m/z=7508 Da.

Table 1. Reproducibility And Yield of $Au_{30}S(StBu)_{18}$

No	Crude Product Used	*t*-C_4H_9:Toluene for TCT	T (°C)	Time (h)	mg collected from TCT	Au_{30}(S-*tert*-C_4H_9)$_{18}$ Collected (mg)	Date Observed
1	DC1-44-tBSH(I)-3 (46mg)	1:1	70	14	30.1	15.3	10-29-2012
2	DC1-45-tBSH(I)-3 (25.5mg)	1:1	70	2	10.2	2.6	10-29-2012
3	DC1-44-tBSH(I)-3 (10mg)	*0.5mL t-C_4H_9	95	4	Degraded		
4	DC1-45-tBSH(I)-4 (56mg)	2:1	100	3.5	13.5		11-05-2012
5	DC1-48-cbdSEC (37mg)	1:1	70	14	8.8	2.4	11-12-2012
6	DC1-49-tBSH(I)-4 (14mg)	2:1	80	3	9.0	3.9	12-08-2012
7	DC1-50-tBSH(I)-5 (24mg)	2:1	80	1	22.3	5.8	12-08-2012
8	DC1-52-tBSH(I)-6 (13mg)	*1.0mL t-C_4H_9	80	2	10.3	2.3	12-14-2012
9	DC1-52-tBSH(I)-6 (26mg)	1:1	80	2	16.4	2.6	12-14-2012
10	DC1-53-tBSH(I)-6 (37mg)	*1.0mL t-C_4H_9	90	0.5	25.7	7.4	12-18-2012
11	DC1-69-tBSH(I)-7 (14mg)	4:1	80	3	5.4	2.9	02-01-2012
12	DC1-70-tBSH(I)-8 (20mg)	4:1	80	2	14.3	4.8	02-24-2013
13	DC1-70-tBSH(I)-8 (40mg)	4:1	80	2	33.2	7.6	03-07-2013
14	DC1-71-tBSH(I)-8 (25mg)	3:1	95	3	17.0	4.1	03-07-2013
15	DC1-75-tBSH(I)-9 (34mg)	3:1	100	1	24.1	5.5	03-07-2013
16	DC1-82-tBSH(I)-8,9cbd (58mg)	3:1	110	2	36.5	9.2	03-09-2013
17	DC1-85-tBSH(I)-10 (36mg)	3:1	90	3	21.7	3.8	03-20-2013
18	DC1-86-tBSH(I)-10 (48mg)	2:1	85	24	30.0	5.2	03-26-2013
19	DC1-90-tBSH(I)-11 (62mg)	3:1	80	24	54.3	4.9	04-11-2013
20	DC1-90-tBSH(I)-11 (53mg)	3:1	80	5	41.2	3.8	04-11-2013
21	DC1-94-tBSH(I)-1:2SH (15mg)	3:1	90	4	12.3	4.6	04-26-2013

Table 2. Unit-Cell data for seven different crystals of $Au_{30}S(StBu)_{18}$

Sample Code	**a (Å)**	**b (Å)**	**c (Å)**	**α (°)**	**β (°)**	**γ (°)**	**Volume (Å^3)**	**Crystal System**	**Structure Solved/Presence of *u*-3 Sulfur**
UMCB0042	14.9	19.9	28.1	81.0	78.7	70.2	7680	Triclinic P	Yes/Yes
UMCB0051	14.9	19.8	28.1	81.1	78.6	69.9	7634	Triclinic P	Yes/Yes
UMCB0052	15.1	20.0	28.5	81.2	78.5	70.1	7898	Triclinic P	Yes/Yes
UMCB0055	15.2	20.1	28.5	81.4	78.5	69.8	7966	Triclinic P	Yes/Yes
UMCB0055a	15.0	19.9	28.2	81.4	78.6	69.9	7711	Triclinic P	Yes/Yes
UMCB0059	14.9	19.8	28.1	81.5	78.6	69.7	7575	Triclinic P	Yes/Yes
UMCB0064	14.9	19.7	28.0	81.1	78.6	69.8	7516	Triclinic P	Yes/Yes

CHAPTER IV: RESULTS AND DISCUSSION

Seeking to demonstrate physical alterations and characteristic changes in thiolate-protected gold nanostructures brought forth solely by increasing ligand bulkiness, Tracy's report[10] in 2012 marked the first indication that ligand bulkiness leads to compositional assignments based on mass spectrometry that possess a heightened ratio of gold atoms compared to the number of thiolate ligands required, as well as exhibit Au-S bond strengths more labile as compared to those pertaining to routine thiolate-ligands. Provided by the further evidence from Tsukuda's report of the $Au_{41}(S\text{-}Eind)_{12}$ structure, this heightened gold:thiol ligand ratio was indicative of an alteration in the core geometry. Our report of the $Au_{30}(StBu)_{18}$ composition, for example, in comparison with that of the $Au_{25}(SR)_{18}$ represents an increase of five gold atoms while the number of thiol ligands remains constant; this increase in five gold atoms in the former was expected to be accompanied by a structural change from the latter's known structure of an Au_{13} icosahedron surrounded by six dimeric staples. It was therefore necessary to deduce the spatial arrangement of atoms crystallographically for the structure in order to gain knowledge into the geometrical acquisition of bulky-ligated gold nanomolecular structures.

Shown in figure 12a is the total structure of the $Au_{30}S(StBu)_{18}$ green-gold nanomolecule, first reported isolated and characterized in pure form followed by having the structure solved reported by our lab, with hydrogens omitted for clarity [13]. The structure is based upon an Au_{20} bicuboctahedron (figure 12b), whereby two thirteen-atom cuboctahedra "interpenetrate" into one another, sharing six atoms along the interface and supporting two additional 'hub' atoms that stellate from opposite ends about an inversion center. Shown in figure 12c are the two novel 'trimeric' staple moieties which extend laterally from opposite ends of the molecule, exhibiting $Au_3(StBu)_4$ coordination and housing a total of six gold atoms and eight *tert*-butanethiol ligands. In addition, there are two more gold atoms and four more *tert*-butanethiol ligands found in the two monomeric $Au(StBu)_2$ staples in 12d, as well as six double-bridging thiolate ligands (figure 12e). This gives an overall atom count of thirty gold atoms and eighteen *tert*-butanethiol ligands, as confirmed previously by mass spectrometry. In the crystal structure, however, the refinement suggests the presence of a unique *u*-3 coordinated lone sulfur atom, unique with regards to both the fact that it forms three bonds to gold atoms (instead of two, as observed previously in the case of those structures referred to as 'routine').

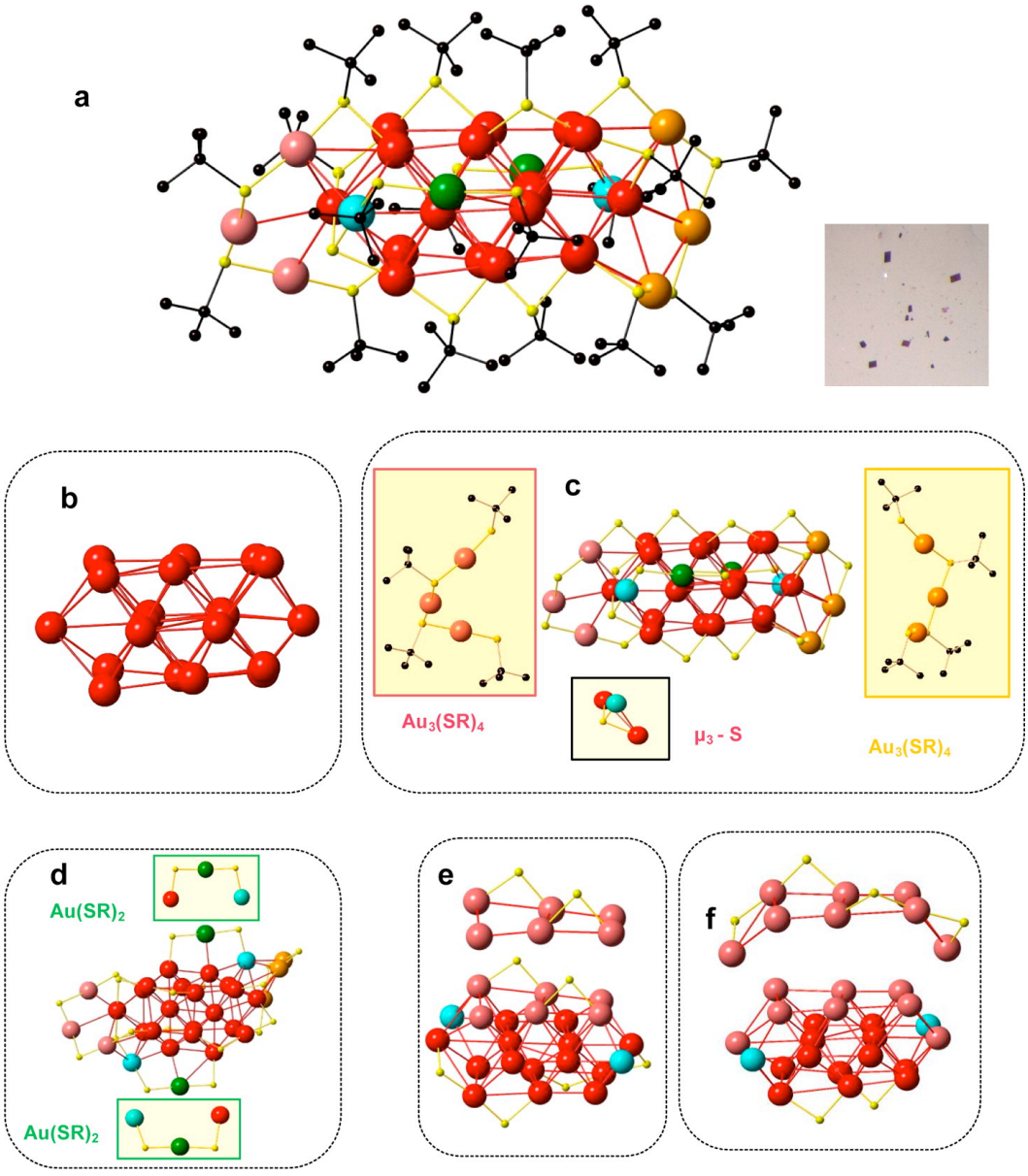

Figure 12. Structure and constituents of the $Au_{30}S(StBu)_{18}$ green-gold nanomolecule. **a.** Total-structure, with H-atoms omitted for clarity, accompanied by a photograph of the rhombic plate-crystals as observed under the microscope. **b.** Au_{20} bicuboctahedron fcc gold core **c.** location and placement of the two trimeric $Au_3(StBu)_4$ staple units, as well as the unique *u*-3 sulfur atom **d**. location and placement of the two monomeric $Au(StBu)_2$ staple units **e, f**. sites of the bridging-ligands above and below the plane of the molecule

The acquisition of the lone "19th sulfur atom is unique not only for the fact that it exists in coordination with the gold core as a lone sulfur atom with no alkyl group, but also because of the u_3-coordination (3 Au-S bonds) of the sulfur atom. Shown below in figure 13, this marks the first incidence of u_3-coordinated sulfur atoms in the Au-SR system; u_3-Sulfur coordination was previously reported in one study regarding Ag-S chemistry [14].

There are two trimeric units with S-Au-S-Au-S-Au-S coordination ($Au_3(StBu)_4$ extending from opposite ends of the core. Their structures are shown in figure 13, whereby they serve as "capping" agents on either of the two ends, preventing any further growth. Novel to the Au-SR system in our report, these trimeric moieties have also been observed in a later report of the $Au_{23}(SCy)_{16}$ nanomolecule, where SCy=cyclohexanethiol; this particular structure is fixated upon a single Au_{13} cuboctahedron.

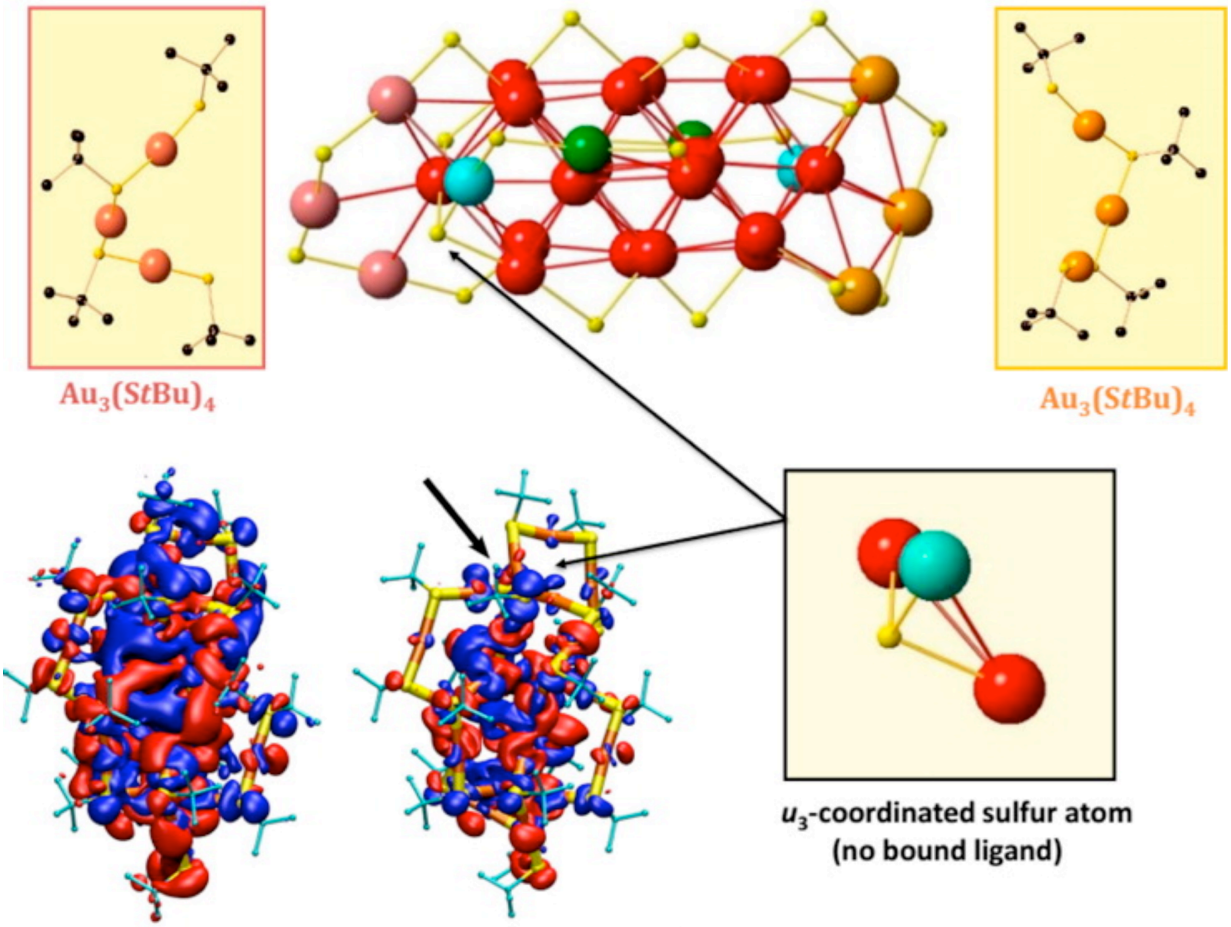

Figure 13. Novel Characteristics of $Au_{30}(StBu)_{18}$. The two novel trimeric staple moieties are shown at the top on either side of the structure. Shown below, at the bottom right, is the lone "19th" Sulfur atom's position within the atomic arrangement above, as well as to the left within the local density structure for the 620 nm feature in the absorbance spectrum of the $Au_{30}S(StBu)_{18}$. The local density of the respective composition is accompanied by the closely related $Au_{30}(StBu)_{18}$ green-gold molecule adjacent to it.

Originally, the adoption of a lone sulfur atom with no bound ligand in the composition given by X-ray crystallography was thought to be instrumental error. However, it was later concluded by our co-workers, along with ourselves, that the acquisition is a result of the forces governing the crystallization of the material into the solid state from the mother liquor. It was not only until after the report in *JACS* [13] came out that the following experiment was conducted; pure $Au_{30}(StBu)_{18}$ was collected after two successive separation runs through the Size-Exclusion Chromatogram to purify the material. After transferring into two 4 mL-screw cap vials and drying the THF solvent via rotary-evaporation, 3 mL of toluene was added to each vial; one vial was then purged fifteen minutes with O_2 gas, and one with N_2-gas in order to determine if an oxidation is the cause of this lone-sulfur atom's adoption into the geometry. These two vials were then allowed to sit for seven days within an ethanol-insoluble layer bath for vapor-vapor diffusion crystal growth. The top spectrum shown below in figure 14 represents the ESI-MS positive mode data collection of the rhombic plate-crystals (picture inset) observed in high yield in the oxygen-purged growth medium. The asterisk denotes the 1+ charge state of $Au_{30}(StBu)_{18}$ at an m/z=7514, shown additionally in the green spectrum on the bottom of figure 14, which represents the ESI-MS positive mode data collection for the nitrogen-purged growth medium.

The rod-like crystals shown in the inset were observed for the crystals grown in an oxygen-free environment and, remarkably, showed an absence of the peak for $Au_{30}S(StBu)_{18}$. This is illustrated by the dollar sign ($) in the top spectrum at an m/z=7547; it was therefore concluded that the acquisition of the lone 19th sulfur atom is a result of an oxidation. It remains to yet be known as to why the *tert*-C_4H_9 is cleaved.

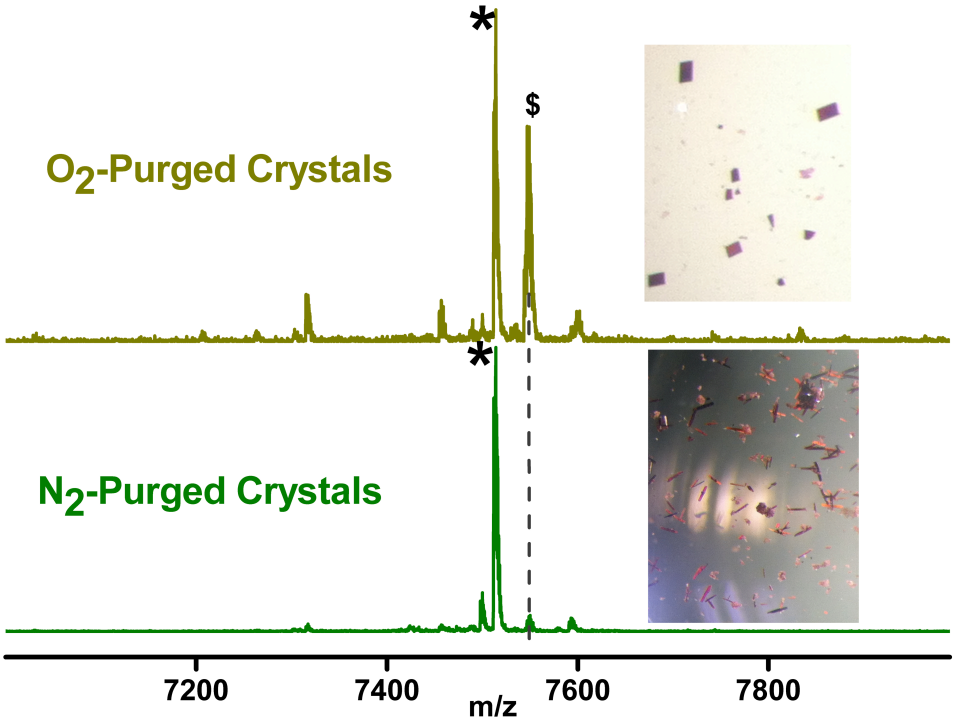

Figure 14. ESI 1+ charge regions for N_2 vs. O_2 purged-crystals 1+ charge region for the rhombic plate crystals grown in an O_2 media, which show an intense peak for the acquisition of the 19th Sulfur atom at m/x=7547, absent in the bottom spectrum for the rod-like crystals grown in an N_2 medium (bottom)

CHAPTER V: CONCLUSION

The findings made by the student and presented in this account highlight the results of the determination of the bulky-ligand induced transformation from icosahedron-based Au nanomolecules to octahedran-based geometries. The transformation is evident through the determination of the crystal structure of $Au_{30}(SR)_{18}$ by the student, as compared with the previous report of $Au_{25}(SC_2H_4\text{-}Ph)_{18}$. Based on the fact that there are five additional gold atoms in the former compared to the latter, while the number of ligands remains constant, it is clear that a change in atomic structure accompanies the change in composition. The structural alteration itself is shown below, whereby the thirteen gold atoms comprising the core of Au_{25} is shown on the left. Shown on the right are the twenty gold atoms located in the fcc bicuboctahedron core.

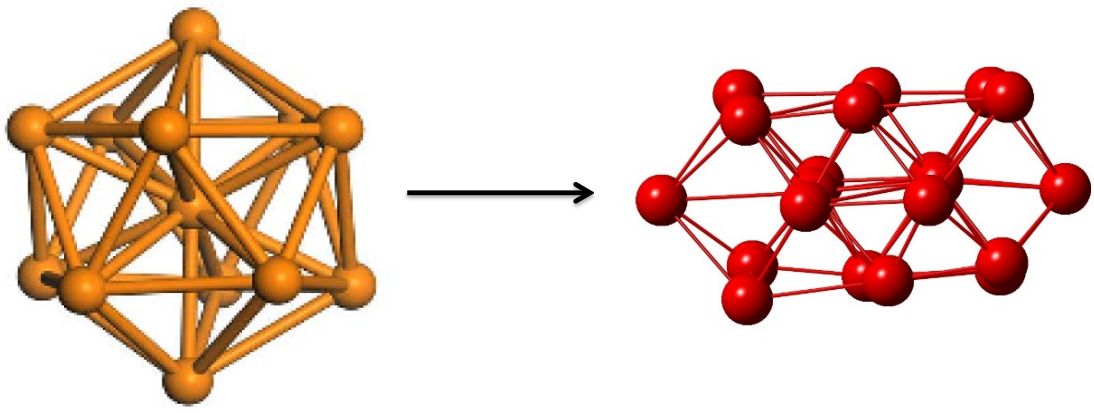

Figure 15. Structural Transformation Upon Bulky Thiolate Ligation of Au Nanomolecules. Shown on the left is the Au_{13} icosahedron of $Au_{25}(SR)_{18}$ and on the right is the Au_{20} bicuboctahedron of $Au_{30}(SR)_{18}$

Figure 15 outlines the induced transformation of the underlying geometry stabilizing the nanomolecule as an entire entity as a result of the application of bulky thiolate ligands on the surface monolayer. Shown on the left in figure 15 is the Au_{13} icosahedron gold core, characteristic to the $Au_{25}(SPhC_2H_4)_{18}$ nanomolecule. The eighteen phenylethanethiol stabilizing-ligands permit for even-spacing and a reduced degree of steric hindrance upon the surface; however, upon the application of bulky, sterically-hindered thiolate ligands, the heightened level of crowding between neighboring ligands on the surface gives way to a conformational change in the 3-dimensional geometry from the icosahedron to face-center cuboidal (fcc) cuboctahedron-based derivatives.

Our work has led to the discovery of novel aspects concerning the acquisition of a particular 3-Dimensional arrangement of the gold atoms and thiolate ligands that coordinate to form an overall nanomolecular entity. With regards to the $Au_{30}S(StBu)_{18}$ nanomolecule, experimentally resolved on a *Bruker Apex* to 1.12 Å, the protecting layer revealed three new aspects: trimeric $Au_3(StBu)_4$ staples, double-bridging u_2-thiolate ligands, and a lone sulfur atom in u_3-coordination. Additionally, our work provides a close-comparison of closely related nanomolecules in structure pertaining to chirality. $Au_{28}(SPh\text{-}tBu)_{20}$, shown below in figure 16, is also based upon an Au_{20} fcc bicuboctahedron; the clockwise enantiomer is shown below in comparison to that of the calculated DFT-structure of $Au_{30}(StBu)_{18}$.

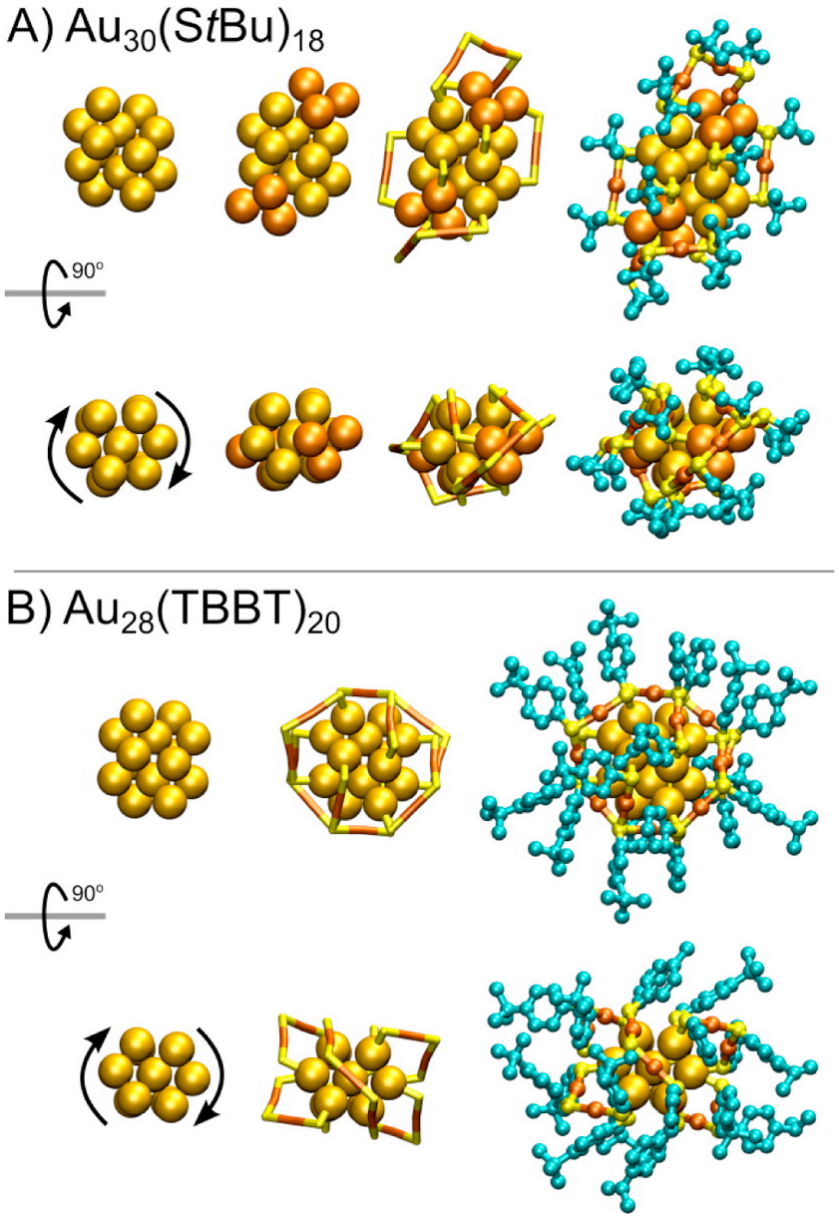

Figure 16. Structural comparison of A) $Au_{30}(StBu)_{18}$ and B) $Au_{28}(SPh\text{-}tBu)_{20}$. The clockwise Au_{14} enantiomer is shown, which forms the nucleus of the Au_{20} bicuboctahedron gold core, which is chiral in the case of both species. Also shown is the orientation of the staples and bridging-ligands, illustrating the resemblance between the two.

Additionally, the position of the lone u_3-coordinated sulfur atom at the end of the core in $Au_{30}S(StBu)_{18}$ is analogous to one of the trimeric protecting units found on $Au_{28}(SPh\text{-}tBu)_{20}$. Shown below in figure 17 is the computed Circular Dichroism spectrum for $Au_{30}S(StBu)_{18}$ and $Au_{30}(StBu)_{18}$. The low energy features, displayed above 500 nm on the spectrum, are essentially identical to that of $Au_{28}(SPh\text{-}tBu)_{20}$ as a result of their identical chiral cores.

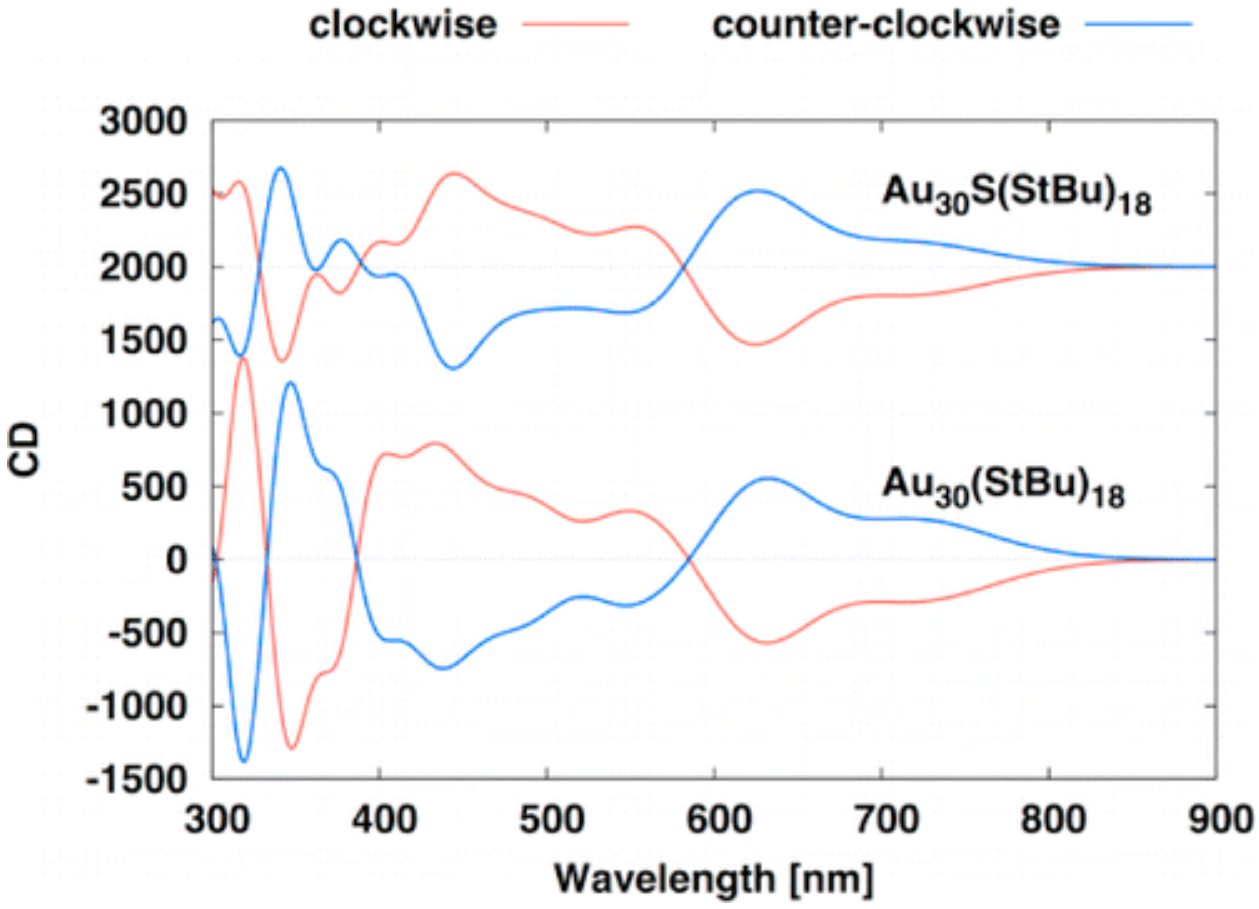

Figure 17. Calculated CD spectrum for the two enantiomers of the $Au_{30}S(StBu)_{18}$ and $Au_{30}(StBu)_{18}$ structures. The spectra were calculated based on the crystal structure of $Au_{30}S(StBu)_{18}$, shown on top, used in order to acquire the DFT-structure for $Au_{30}(StBu)_{18}$ below

BIBLIOGRAPHY

1. Dharmaratne, A.; Dass, A.; *Phys. Chem.*, **2010**, *12*, 11785-11790
2. Heuer-Jungemann, A.; Harimech, P.; Brown, T.; Kanaras, A.; *Nanoscale*, 2013, **5**, 9503-9510
3. Zhou, X.; Xu, W.; Liu, G.; Panda, D.; Chen, P.; *J. Am. Chem. Soc.*, 2009, **132**, 138-146
4. Han, G.; Ghosh, P.; Rotello, V.; *Nanomedicine*, 2007, **2**, 113-123
5. Heaven, M.; Dass, A. White, P.; Holt, K.; Murray, R.W.; *J. Am. Chem. Soc*, **2008**, *130*(12), 3754-3755
6. Qian, H.; Eckenhoff, W.; Zhu, Y. Pintauer, T.; Jin, R.; *J. Am. Chem. Soc.*, **2010,** *132(24)*, 8280-8281
7. Jadzinsky, P.; Calero, G.; Ackerson, C.; Bushnell, D.; Kornberg, R.; *Science*, **2007**, *318*, 430-433
8. Hakkinen, H.; *Nature*, **2012**, *4*, 443-455
9. Zeng, C.; Qian, H.; Li, T.; Li, G.; Rosi, N.; Yopon, B.; Barnett, R.; Whetten, R.; Landman, U.; Jin, R.; *Angew. Chem. Int. Ed.*, **2012**, *51*, 13114-13118
10. Krommenhoek, P.; Wang, J.; Hentz, N.; Johnston-Peck, A.; Kozek, K.; Kalyuzhny, G.; Tracy, J.; *ACS Nano*, **2012**, *6*(6), 4903-4911
11. Nishigaki, J.; Tsunoyama, R.; Tsunoyama, H.; Ichikuni, N.; Yamazo, S.; Negishi, Y.; Ito, M.; Matsuo, T.; Tamao, K.; Tsukuda, T.; *J. Am. Chem. Soc.*, **2012**, *134*(35), 14295-14297
12. Crasto, D.; Dass, A.; *J. Phys. Chem. C*, **2013**, *117*(42), 22094-22097
13. Crasto, D.; Malola, S.; Brosofsky, G.; Dass, A.; Hakkinen, H.; *J. Am. Chem. Soc.*, **2014**, *136*(13), 5000-5005
14. Mo, L.-Q.; Jia, J.-H.; Sun, L.-j.; Wang, Q.-M.; *Chem. Commun.*, **2012**, *48*, 8691–8693
15. Zeng, C.; Li, T.; Das, A.; Rosi, N.; Jin, R.; *J. Am. Chem. Soc.*, **2013**, *135*(27), 10011-10013

LIST OF APPENDICES

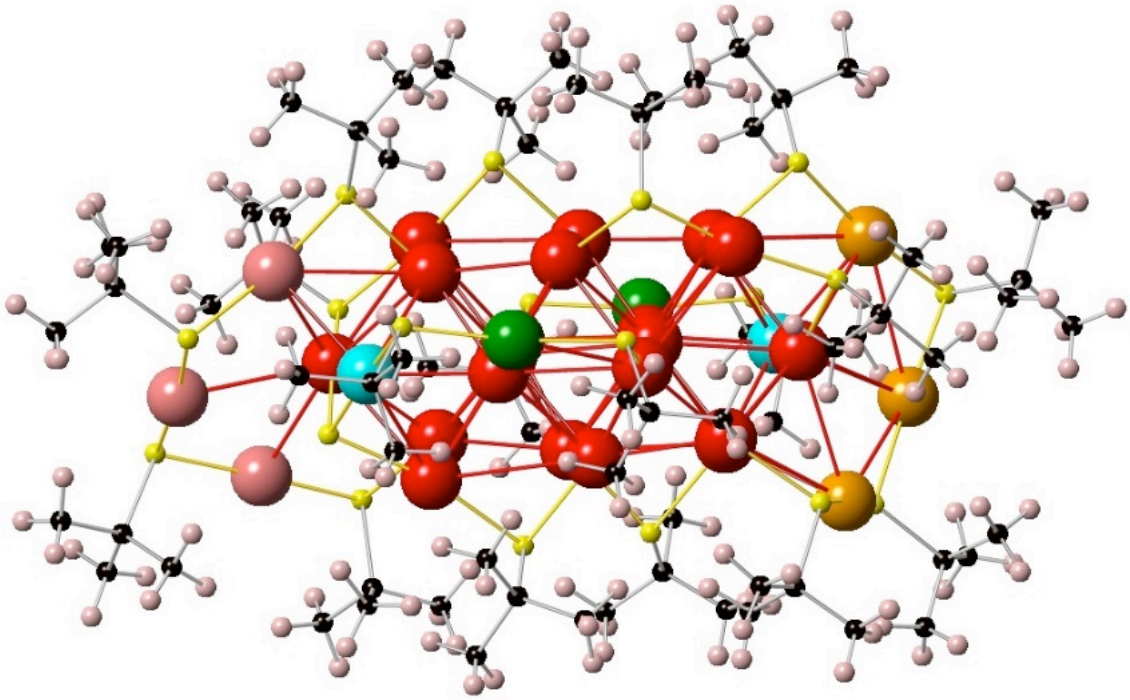

Figure A-1. Total Structure of the $Au_{30}S(StBu)_{18}$ green-gold nanomolecule. Hydrogen atoms are included, displayed in connectivity with the carbon atoms (black) of the *tert*-C_4H_9 "bulky" alkyl group.

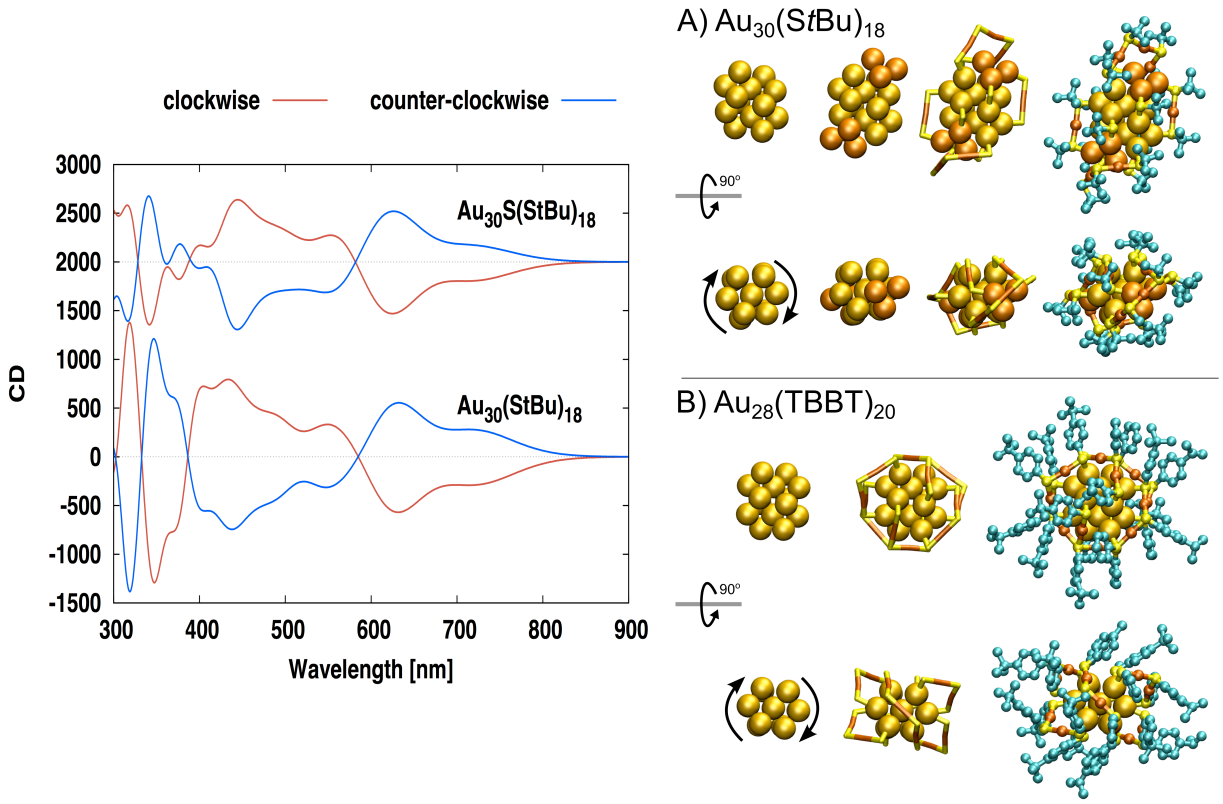

Figure A-2. Circular Dichroism and Enantiomeric Activity. Shown on the left is the theoretically-calculated model of the circular dichroism spectra of $Au_{30}S(StBu)_{18}$ on top and $Au_{30}(StBu)_{18}$ on bottom. Based on this, it is clear that both unit cells contain left- and right-handed enantiomers (mirror images). Shown on the right is the comparison of the chirality of $Au_{30}(StBu)_{18}$ in A) (top) compared to the closely-related $Au_{28}(STBBT)_{20}$, where STBBT=*tert*-butylbenzenethiol [15]. This structure, shown on the bottom in B), is also based upon an Au_{20} bicuboctahedron core and, while additionally exhibiting enantiomeric character in the unit cell, allowed for the first analysis of two closely-related structures which differed solely upon connectivity on the monolayer

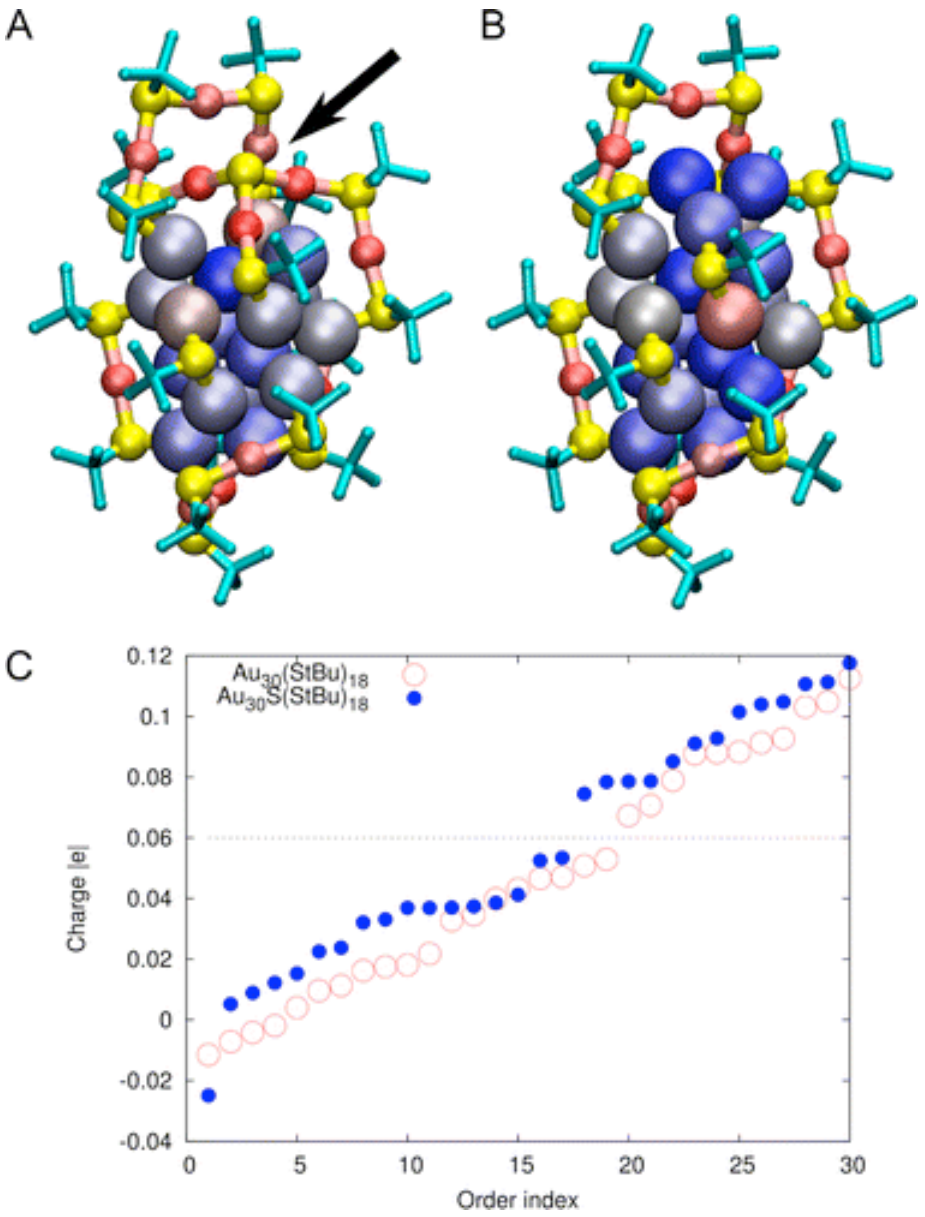

Figure A-3. Bader charge analysis on the total structure of $Au_{30}S(S\text{-}t\text{-}Bu)_{18}$ (A) and the DFT-derived structure of $Au_{30}(StBu)_{18}$ (B). The "19th sulfur" is shown by the arrow in (A). Colors of atoms, *t*-Bu blue sticks, sulfur yellow, gold in ranging colors from blue (negative) to red (positive) according to the DFT charge analysis as follows: (A) from –0.025|e| to +0.118|e|, (B) from –0.012|e| to +0.113|e|. The "19th sulfur" in (A) has the charge of –0.32|e|. Both clusters have a clockwise chiral core shown also in Figure 3. (C) Charges of Au-atoms ordered from the lowest to the highest. A stepwise change in the charge of the atoms is shown as a dashed line.

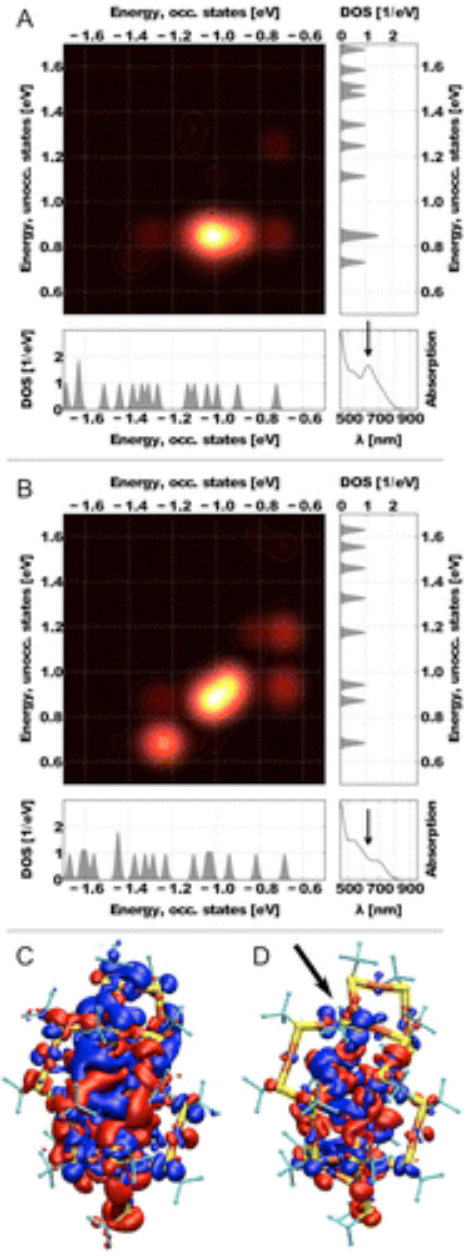

Figure A-4. Transition contribution map (TCM) for the 630 nm feature in (A) $Au_{30}(S\text{-}t\text{-}Bu)_{18}$ and (B) $Au_{30}S(S\text{-}t\text{-}Bu)_{18}$. The most intensive transitions are seen from the HOMO–2 state to the LUMO+1 and LUMO+2 states in both of the clusters. The nature of these Kohn–Sham states is consistent between the clusters. Induced densities solved for the feature at 630 nm for (C) $Au_{30}(S\text{-}t\text{-}Bu)_{18}$ and (D) $Au_{30}S(S\text{-}t\text{-}Bu)_{18}$. The positions of the "19th sulphur" is shown by the arrow in (D).

checkCIF/PLATON report
Structure factors have been supplied for datablock(s): **sep9**
{THIS REPORT IS FOR GUIDANCE ONLY. IF USED AS PART OF A REVIEW PROCEDURE FOR PUBLICATION, IT SHOULD NOT REPLACE THE EXPERTISE OF AN EXPERIENCED CRYSTALLOGRAPHIC REFEREE.}
No syntax errors found. CIF dictionary

Datablock: sep9
Bond precision: C-C = 0.0470 A
Cell: Temperature: 100K
Interpreting this report
Wavelength=0.71073
a=14.982(5) alpha=81.352(7) beta=78.546(6) gamma=69.930(7) 173 K
Reported 7713(5) P -1 -P 1 C72 H162 Au30 S19 C72 H162 Au30 S19 7546.14 3.249
28.681 6536.0
14,18,26 13890 0.037,0.087
Calculated 7713(5) P -1 -P 1
Volume Space group Hall group Moiety formula Sum formula Mr Dx,g cm-3 Z22
Mu (mm-1) F000 F000' h,k,lmax Nref Tmin,Tmax Tmin'
28.680 6536.0 6439.81 14,18,26 13957 0.036,0.267 0.010
C72 H162 Au30 S19 C72 H162 Au30 S19 7546.40 3.249
Correction method= MULTI-SCAN Data completeness= 0.995 R(reflections)= 0.0590(8334) S = 1.039 Npar= Npar = 784
b=19.899(7) c=28.215(10)
Theta(max)= 19.782 wR2(reflections)= 0.1970(13890)

The following ALERTS were generated. Each ALERT has the format **test-name_ALERT_alert-type_alert-leve**l.

Click on the hyperlinks for more details of the test.

Alert level A

THETM01_ALERT_3_A The value of sine(theta_max)/wavelength is less than 0.550 Calculated sin(theta_max)/wavelength = 0.4762

Author Response: The data were collected to a 0.8 A resolution, however were truncated at 1.2 A due to the weakness of the high angle data. The cutoff threshold for R(sym) and mean I/sigma was set to be 0.45 and 2.0, respectively.

PLAT201_ALERT_2_A Isotropic non-H Atoms in Main Residue(s) ..... 72 Why ?

Author Response: An anisotropic refinement of all non-H atom was investigated, but it was not computationally stable. The numerical refinement indicators did not show substantial improvement and the isotropic model was retained to conserve the data. The data was truncated at 1.2 A.

PLAT602_ALERT_2_A VERY LARGE Solvent Accessible VOID(S) in Structure ! Info

Author Response: The structure contains two solvent accessible voids of 1850 and 524 A3 that contain a calculated 1729 and 509 e for the diffusely diffracting species respectively. Attempts to identify and model the possible counterion and solvent molecules were not successful. Alternative approaches to account for the diffusely diffracting species (option SQUEEZE of program PLATON and the Maps->Mask option in OLEX2 did not produce an improved refinement. These routines are not believed to work with large clusters. Whereas it is possible to assign partial occupancies to atoms that would represent atoms in the solvents no sensible model was obtained and the choice was made to ignore these peaks.

VITA

DAVE CRASTO
4030 Dogwood Drive Jackson, MS 39211 601-613-7424 dwcrasto@go.olemiss.edu

EDUCATION

M. S., Chemistry, University of Mississippi, December 2014
Concentrations: Analytical Chemistry, Gold Nanomaterials
Thesis: Structural Analysis of Bulky Thiolate-Protected Gold Nanomolecules

B.A., Chemistry & Psychology, University of Mississippi, December 2012

TEACHING EXPERIENCE

Teaching Assistant, 2011-2014
University of Mississippi
Course: Laboratory of General Chemistry

PUBLICATIONS

Crasto, D.; Dass, A.; *J. Phys. Chem. C*, **2013**, 117, 22094-22097

Crasto, D.; Malola, S.; Brosofsky, G.; Dass, A.; Hakkinen, H.; *J. Am. Chem. Soc.*, **2014**, 136(13), 5000-5005

Crasto, D.; Barcaro, G.; Stener, M.; Sementa, L.; Fortunelli, A.; Dass, A.; *J. Am. Chem. Soc.,* **2014**, 136(42), 14933-14940